Shared vulnerability for connectome alterations across psychiatric and neurological brain disorders

de Lange, Siemon C; Scholtens, Lianne H; van den Berg, Leonard H; Boks, Marco P; Bozzali, Marco; Cahn, Wiepke; Dannlowski, Udo; Durston, Sarah; van Haren, Neeltje E M; Hillegers, Manon H J; Koch, Kathrin; Meinert, Susanne; Ophoff, Roel A; Repple, Jonathan; Kahn, René S; van den Heuvel, Martijn P

published in
Nature Human Behaviour
2019

DOI (link to publisher)
10.1038/s41562-019-0659-6

document version
Peer reviewed version

Shared vulnerability for connectome alterations across psychiatric and neurological brain disorders

Siemon C. de Lange[1], Lianne H. Scholtens[1], Alzheimer's Disease Neuroimaging Initiative, Leonard H. van den Berg[2], Marco P. Boks[3], Marco Bozzali[4,5], Wiepke Cahn[3, 6], Udo Dannlowski[7], Sarah Durston[3], Elbert Geuze[3,8], Neeltje E.M. van Haren[3,9], Manon H.J. Hillegers[3,9], Kathrin Koch[10,11], María Ángeles Jurado[12,13,14], Matteo Mancini[15,16], Idoia Marqués-Iturria[12], Susanne Meinert[7], Roel A. Ophoff[17,18], Tim J. Reess[10], Jonathan Repple[7], René S. Kahn[19] and Martijn P. van den Heuvel[1,20,*]

[1] Connectome Lab, Department of Complex Trait Genetics, Center for Neurogenomics and Cognitive Research, Vrije Universiteit Amsterdam, Amsterdam Neuroscience, Amsterdam, The Netherlands

[2] UMC Utrecht Brain Center, Department of Neurology, University Medical Center Utrecht, Utrecht, The Netherlands

[3] UMC Utrecht Brain Center, Department of Psychiatry, University Medical Center Utrecht, Utrecht, The Netherlands

[4] Department of Neuroscience, Brighton and Sussex Medical School, University of Sussex, Brighton, East Sussex, UK

[5] Neuroimaging Laboratory, Santa Lucia Foundation IRCCS, Rome, Italy

[6] Altrecht Science, Altrecht Mental Health Institute, Utrecht, The Netherlands

[7] Department of Psychiatry, University of Muenster, Muenster, Germany

[8] Brain Research and Innovation Centre, Ministry of Defence, Utrecht, The Netherlands

[9] Department of Child and Adolescent Psychiatry/Psychology, Erasmus University Medical Center - Sophia Children's Hospital, Rotterdam, The Netherlands

[10] Department of Neuroradiology & TUM-Neuroimaging Center (TUM-NIC), School of Medicine, Klinikum rechts der Isar, Technische Universität München, Munich, Germany

[11] Graduate School of Systemic Neurosciences GSN, Ludwig-Maximilians-Universität, Biocenter, Munich, Germany

[12] Departament de Psicologia Clínica i Psicobiologia, Universitat de Barcelona, Barcelona, Spain

[13] Institut de Neurociències, Universitat de Barcelona, Barcelona, Spain

[14] Institut de Recerca Pediàtrica Hospital Sant Joan de Déu (IRSJD). Barcelona, Spain

[15] Clinical Imaging Sciences Centre, Brighton and Sussex Medical School, Brighton, United Kingdom
[16] Centre for Medical Image Computing, Department of Medical Physics and Biomedical Engineering, University College London, London, United Kingdom
[17] Center for Neurobehavioral Genetics, University of California Los Angeles, Los Angeles, USA
[18] Department of Psychiatry, Erasmus MC University Medical Center, Rotterdam, The Netherlands
[19] Department of Psychiatry and Behavioral Health System, Icahn School of Medicine at Mount Sinai, New York, USA
[20] Department of Clinical Genetics, Amsterdam UMC, Vrije Universiteit Amsterdam, Amsterdam Neuroscience, Amsterdam, The Netherlands

* Corresponding authors: Martijn P. van den Heuvel (martijn.vanden.heuvel@vu.nl; ORCID: http://orcid.org/0000-0003-1570-1195)

Abstract

Macroscale white matter pathways are the infrastructure for large-scale communication in the human brain and a prerequisite for healthy brain function. Disruptions in the brain's connectivity architecture play an important role in many psychiatric and neurological brain disorders. Here we show that connections important for global communication and network integration are particularly vulnerable to brain alterations across multiple brain disorders. We report on a cross-disorder connectome study comprising in total 1,033 patients and 1,154 matched controls across eight psychiatric and four neurological disorders. We extracted disorder connectome fingerprints for each of these twelve disorders and combined them into a 'cross-disorder disconnectivity involvement map' describing the level of cross-disorder involvement of each white matter pathway of the human brain network. Network analysis revealed connections central to global network communication and integration to display high disturbance across disorders, suggesting a general cross-disorder involvement and importance of these pathways in normal function.

Main

The macroscale connectome is the brain's anatomical network for global communication and multimodal integration of information between brain areas [1]. Topologically central connections have been argued to provide benefits for global neural integration [2] and healthy brain function [3]. Due to

their high biological cost, these central connections may also be prone to a wide range of disease mechanisms [1].

Disease-associated alterations in structural and functional brain connectivity play a role in a wide range of psychiatric and neurological conditions (see for a brief overview Supplementary Note). Potentially, these disconnectivity patterns converge across disorders to a substrate of connections that are generally vulnerable to disease effects. Such convergence is supported by observations that multiple neuropsychiatric disorders overlap in their involved functional neural circuits [4], their genetic risk factors [5] and their symptomatology [6]. Meta-analyses of MRI studies have indicated high overlap in structural brain phenotypes and have suggested widespread anatomical and functional changes in densely connected 'hub regions' [7]. So far, disease connectome investigations have been focused on the examination of brain disconnectivity in single or small sets of disorders, and lack power to identify cross-disorder biological patterns of white matter disconnectivity [8]. A cross-disorder disease-integrative approach provides opportunities to assess potential general vulnerability of connections in the human brain and gain insight into biological mechanisms shared across brain disorders [8].

In this study, we performed a cross-disorder connectome analysis, integrating connectivity data across twelve brain disorders, comprising diffusion MRI data of in total 1,033 patients and 1,154 matched controls, across eight psychiatric conditions (schizophrenia, bipolar disorder, attention deficit hyperactivity disorder, autism spectrum disorder, major depressive disorder, obesity, obsessive-compulsive disorder, posttraumatic stress disorder) and four neurological disorders (Alzheimer's disease, its prodromal stage mild cognitive impairment, amyotrophic lateral sclerosis and primary lateral sclerosis). A 'cross-disorder involvement map' was constructed by combining derived 'disconnectivity maps' across the twelve conditions, identifying potential circuitry and network properties that play a general role in multiple disorders. We further combine cross-disorder involvement maps with results from network analysis of the human connectome, anatomical data and functional mappings of brain regions and functions. We show that connections important for neural integration and cognitive brain function are disproportionately involved across multiple brain disorders.

Results

Cross-disorder involvement map

We examined diffusion MRI data of patients and controls across twelve brain disorders from previously published studies and cohorts (listed in Supplementary Method 1). Connectome maps were reconstructed by computing the level of connectivity between 219 distinct cortical brain regions (depicted by a subdivision of the Desikan-Killiany atlas, DK-219). Validation results using different parameter settings and different subparcellations of the Desikan-Killiany atlas (e.g. DK-114) are presented in the Supplementary Result 1. Patient-control matching was performed per dataset (to ensure group-wise matching of age and gender, see Supplementary Method 2) and after quality control of the data (see Supplementary Method 2) 1,033 patients and 1,154 matched controls were included for group analysis. An overview of the demographics is provided in Supplementary Figure 1 and Table 1. Differences in connectivity strength (measured by fractional anisotropy) between patient and controls were computed for all connections in each disorder separately, and then combined into disorder disconnectivity maps (Figure 1A). In each disorder, a fixed number of connections (top 15%) with highest disconnectivity effects was selected as 'disorder involved', ensuring equal presence of all disorders in the final cross-disorder involvement map (validation of other settings (5% - 25%) and an alternative selection-free meta-analysis strategy, yielded similar effects, see Supplementary Result 2 and Supplementary Result 3). Disease maps were combined in a 'cross-disorder disconnectivity involvement map' depicting across all twelve disorders, per connection, the percentage of disorders in which that connection was found to be affected (Figure 1B).

We next performed network-based statistics (NBS, see Methods for details, [9]), a method that identifies subnetworks of edge-wise effects. We examined the subnetworks of connections with high cross-disorder involvement, comparing the observed subnetwork size with a null-distribution of random cross-disorder involvement observed when patients and controls are shuffled (10,000 permutations). NBS analysis revealed four significant clusters of connections with high cross-disorder involvement (among the set of connections involved in NBS threshold >30%, >40% and >45% of the disorders, all $p < 0.05$, Supplementary Figure 2), with the largest subnetwork containing 80 regions and 216 connections, including superior frontal, central, posterior, and parietal regions ($p < 0.001$, Figure 1E).

We continued by examining white-matter vulnerability from a neuroanatomical perspective, examining cross-disorder involvement of 38 major cortico-cortical white matter bundles parcellated

according to the ICBM-DTI-81 white matter atlas (see Methods). Significantly high levels of cross-disorder involvement were observed in the body and splenium of the corpus callosum (body: $p = 0.008$; splenium: $p < 0.001$), superior corona radiata (left: $p = 0.008$; right: $p < 0.001$) and posterior corona radiata (left: $p = 0.008$; right: $p = 0.015$, one-sided permutation testing, 10,000 permutations, Bonferroni corrected for multiple testing across 38 tracts).

Region-wise cross-disorder involvement

Averaging cross-disorder involvement across connections of each cortical area provided a measure of region-wise cross-disorder involvement (Figure 1D). We associated this region-wise cross-disorder involvement with cortical activation patterns associated with cognitive brain functions obtained from the NeuroSynth database. Region-wise cross-disorder involvement showed to be positively associated with brain functions related to movement, attention and cognitive control, including low-level functions such as 'eye movement' (Pearson's $r(217) = 0.31$, $p < 0.001$, 95% CI = 0.18-0.42) and 'motor' ($r(217) = 0.21$, $p = 0.025$, 95% CI = 0.09-0.34), as well as high-level functions such as 'cognitive control' ($r(217) = 0.28$, $p < 0.001$, 95% CI = 0.15-0.40), 'cued attention' ($r(217) = 0.28$, $p < 0.001$, 95% CI = 0.16-0.40) and 'visual attention' ($r(217) = 0.25$, $p = 0.004$, 95% CI = 0.12-0.37) (Bonferroni corrected for multiple testing across 24 functions, see Supplementary Figure 3 and for a complete list of functions Supplementary Table 1).

Edge-wise centrality measures

We further investigated the vulnerability of connections and their contribution to local and global communication in the brain network. The topological role of connections was assessed using four edge-wise centrality measures computed on a reference connectome that was based on high-resolution data from the Human Connectome Project (HCP) [10]. We used HCP data to ensure that the computation of network measures was performed independently from any patient-control effects and any of the included disorder datasets. The contribution of a connection in global communication across the network was measured by means of 'edge betweenness centrality', which assesses the number of shortest topological paths through each connection. Connections with high betweenness centrality (top 25%, n = 290) were found to be significantly more involved across disorders as contrasted to subject-label permuted cross-disorder involvement maps ($d = 0.41$, one-sided permutation testing, 10,000 permutations, $p < 0.001$, Figure 2, see Methods). In contrast, no significant effect was observed in connections with a low betweenness centrality (lowest 25%, n = 290, $p = 1.000$). We further examined an extended definition of global network integration by means of 'network communicability', a metric which takes into account all possible communication paths between nodes in the network [11]. Brain connections that contribute the most to brain network

communicability (top 25%, n = 290) again showed significantly higher cross-disorder involvement (d = 0.18, p = 0.009), suggesting disproportional disease vulnerability in connections central to global brain communication. In contrast, connections with a strong contribution to local network organization (measured by network clustering, n = 290) did not show a predisposition for cross-disorder involvement (p = 0.911). Finally, taking into account the projection distance of network connections (i.e. the physical length of connections in the human brain) also revealed higher cross-disorder involvement among spatially long connections (top 25%, >50 mm, n = 290) in comparison with permuted disconnectivity effects (d = 0.62, p < 0.001, see Methods).

Rich club organization

We next investigated cross-disorder involvement in relation to hub and rich club organization of the human brain network [12]. Densely connected hub regions in the human brain have been suggested to form a centrally connected 'rich club' with high levels of interconnectivity between hub regions, together forming system circuitry that may act as a central backbone for global communication and integration of information [13]. Brain hubs were taken as the top 13% connected regions in the HCP reference connectome (Supplementary Figure 4), and network connections were categorized into rich club connections (7.6% of connections, n = 88) describing connections spanning between hub regions, feeder connections (27.7%, n = 321), describing connections spanning between hub and peripheral regions and local connections (64.7%, n = 751), describing connections spanning between peripheral regions. Significantly disproportionate cross-disorder involvement was observed among rich club connections as compared with local connections (d = 0.43, p < 0.001, one-sided permutation testing, 10,000 permutations, Figure 3) and as compared with feeder connections (d = 0.28, p = 0.013). Feeder connections also showed higher cross-disorder involvement compared with local connections (d = 0.16, p = 0.009).

Global white matter

Widespread white matter differences in fractional anisotropy are often reported in psychiatric and neurological conditions (for a review, see [14]) and could result in a general pattern of reduced connectivity across the connectome. To verify that a cross-disorder vulnerability of central connections is relatively independent from such global white matter changes, we compared the level of cross-disorder involvement of central connections with a null-distribution based on cross-disorder involvement maps obtained by subject-label permutation, in which, per disease and per dataset, the global connectivity strength distribution across patient and control groups was preserved (see Methods). Using this alternative null-condition that controls for global changes in connectivity strength, connections with high betweenness centrality were again found to show

significantly higher cross-disorder involvement (n = 290, d = 0.36, p < 0.001, one-sided permutation testing, 10,000 permutations), indicative of these effects to go beyond disease related global fractional anisotropy changes. Furthermore, connections that contribute the most to brain network communicability also showed significantly higher cross-disorder involvement (n = 290, d = 0.16, p = 0.012). In contrast, connections important for local network integration showed no predisposition for cross-disorder involvement (n = 290, p = 0.900). Cross-disorder involvement was also higher among the spatially longest connections (n = 290, d = 0.55, p < 0.001) and central rich club connections also showed significantly higher cross-disorder involvement (n = 88, d = 0.32, p = 0.003).

Psychiatric and neurological disorders

We further investigated connection vulnerability across the separate classes of psychiatric and neurological disorders (see also Supplementary Result 4). Connections central to global integration showed high vulnerability in psychiatric disorders (Supplementary Figure 5). Across neurological disorders, vulnerability of central connections was restricted to spatially long connections and rich club connections (results reported in Supplementary Result 4). Comparing the cross-disorder involvement of central connections of psychiatric and neurological disorders suggested that cross-psychiatric disconnectivity patterns converge more strongly to central connections than disconnectivity patterns in neurological disorders (Supplementary Figure 6, see Supplementary Result 4). Stronger convergence in psychiatric disorders compared to neurological disorders was further suggested by results from NBS analysis that identified subnetworks with high cross-disorder involvement in psychiatric disorders but not in neurological disorders (Supplementary Result 4 and Supplementary Figure 5).

Cross-disorder hyperconnectivity

We further explored patterns of potential 'disease-related increases in connectivity' in patients compared to controls, as a reflection of cross-disorder hyperconnectivity. Using the same procedure as for the cross-disorder disconnectivity involvement map, we constructed a cross-disorder hyperconnectivity map describing for each connection the percentage of disorders in which a connection was found to show increased connectivity (i.e. higher FA in patients as controls). NBS analysis revealed two subnetworks with high cross-disorder involvement (at NBS thresholds > 30% and > 40%, one-sided permutation testing, 10,000 permutations), with the largest significant subnetwork including 58 regions and 132 connections. This network was left lateralized and included connections of the anterior cingulate gyrus, orbital, medial, inferior and medial frontal regions and superior temporal regions (p = 0.026, Figure 4). Subsequent neuroanatomical mapping of cross-disorder hyperconnectivity did not reveal a significant concentration of cross-disorder involvement

to any of the white matter bundles (all $p > 0.05$, one-sided permutation testing, 10,000 permutations, Bonferroni corrected for multiple testing across 38 tracts). Furthermore, functional mapping showed no significant positive correlations between region-wise cross-disorder involvement and functional mappings (all $p > 0.05$, Pearson's correlation, Bonferroni corrected for multiple testing across 24 functions).

We next tested whether peripheral connections possibly showed higher cross-disorder involvement in hyperconnectivity. We found significantly higher cross-disorder hyperconnectivity compared with subject-label permuted cross-disorder hyperconnectivity maps in connections with low betweenness centrality (lowest 25%, $n = 290$, $d = 0.20$, $p = 0.002$) and connections with a relatively low contribution to communicability ($n = 290$, $d = 0.33$, $p < 0.001$). Connections with low clustering did not show a particularly higher cross-disorder hyperconnectivity ($p = 0.132$). Furthermore, higher cross-disorder hyperconnectivity was found to be also particularly concentrated along short-range connections (<8.3 mm, $n = 290$, $d = 0.27$, $p < 0.001$). Local connections ($n = 751$) that displayed a peripheral role in the rich club organization, showed higher cross-disorder hyperconnectivity than more central feeder connections ($n = 321$, $d = 0.19$, $p = 0.003$) or rich club connections ($n = 88$, $d = 0.29$, $p = 0.004$).

Individual disorder maps

To verify that the observed results were not driven by the disconnectivity profile of any included disorder, we performed a leave-one-disorder-out analysis in which we repeated our analyses leaving out one disorder at a time (see Supplementary Result 5). This analysis confirmed high vulnerability of connections important for global integration and higher cross-disorder involvement of rich club connections compared with feeder and local connections (see Supplementary Result 5) and ruled out that the effects were mainly driven by one specific disorder. This generality was further underscored by the observation that at most three of the twelve disorder disconnectivity maps did not contribute to the vulnerability of central connections (Supplementary Figure 7).

The leave-one-disorder-out analysis further provided an opportunity to quantify the overlap of disorder disconnectivity maps and the cross-disorder involvement map. We tested the distribution of disconnectivity for each disorder between disorder-specific connections (affected in zero, one or two disorders of the 11 other disorders, i.e. excluding the examined disorder) and connections commonly affected (in four or more disorders) (Figure 5). Schizophrenia ($d = 0.77$, $p < 0.001$, two-sided permutation testing, 10,000 permutations, Bonferroni corrected for multiple testing across 12 disorders), PLS ($d = 0.71$, $p < 0.001$), ALS ($d = 0.71$, $p < 0.001$), bipolar disorder ($d = 0.42$, $p = 0.001$),

obesity (d = 0.33, p = 0.019), Alzheimer's disease (d = 0.31, p = 0.040) and ASD (d = 0.31, p = 0.035) showed significantly higher disconnectivity in commonly affected connections. MCI (p = 0.073), ADHD (p = 0.193), PTSD (p = 1), MDD (p = 0.767) and OCD (p = 0.152) did not show significant differences. The increased disconnectivity of commonly vulnerable connections in seven out of twelve disorders provides further evidence that the cross-disorder involvement map incorporates disconnectivity patterns that are relatively general across the majority of brain disorders.

Variation analyses

To ensure our results were generalizable and independent of specific parameter settings, reconstruction method or applied analysis, we repeated our analyses with various alternative research design choices. We repeated our analyses using different analysis parameters for the percentage of disorder-involved connections (Supplementary Result 2, Supplementary Figure 8), percentage of central connections (Supplementary Result 6, Supplementary Figure 9) and percentage of hub regions (Supplementary Result 7, Supplementary Figure 10). Different analysis strategies were tested including a second meta-analysis method that averaged weighted disconnectivity effects across disorders (Supplementary Result 3, Supplementary Figure 11). The group connectome map was based on group-thresholding that reduced the number of included false positive connections, but could overrepresent short-range connections in the group connectome map [15]. Therefore, we also repeated our analyses using an alternative grouping method that preserved connection-length and ensured a balanced sampling of short- and long-range connections in the group connectome map [16] (see Supplementary Result 8). To further ensure our findings were not influenced by connection prevalence (i.e. the number of times a connection could be reconstructed in the population reflecting study power), we verified our results examining the subset of most highly consistent connections (see Supplementary Result 9).

Discussion

Our findings suggest that connections central to network integration and communication in the human brain are potential hotspots for white matter disconnectivity across multiple brain disorders. Cross-disorder disconnectivity was examined in 1,033 patients and 1,154 matched controls across a range of eight psychiatric and four neurological disorders and suggest the common involvement of central connections in multiple brain disorders. We note that our findings do not suggest that all disorders involve change to central connections of the brain network, but that central connections are potential common players across multiple disorders, with a potential high vulnerability of these connections to a wide range of disease processes. Our cross-disorder findings provide three lines of

evidence to support such a cross-disorder vulnerability of central connections of the human brain network.

First, edge-wise network measures revealed connections critical for network efficiency and communicability to display high cross-disorder involvement (Figure 2). This result extends earlier reports of affected efficiency of structural networks in for example depression[17] and in Alzheimer's disease, schizophrenia, multiple sclerosis and ALS (see [18] for a review), suggesting that these effects are perhaps not all disease-specific, but potentially more general to brain disorders than previously reported. Furthermore, our results stress the hypothesized importance of efficient integration of information for healthy brain function [19], with disruptions in central connections potentially leading to disproportional effects in brain dysfunction [20].

A second line of evidence for the vulnerability of central connections is the observation of high cross-disorder involvement among connections characterized by long physical distances (Figure 2). A longer projection distance does not necessarily imply topological importance, but following a hypothesized trade-off in brain organization between minimizing wiring-cost and topological integration, connections spanning long physical distances are expected to be extraordinarily beneficial to network topology [1]. This elevated vulnerability of physically long connections is in line with studies reporting affected fiber tracts such as the superior and inferior longitudinal fasciculus in, for example, ADHD [21], ASD [22], OCD [23], and schizophrenia [24]. Post-hoc analysis showed that high cross-disorder involvement of spatially long connections is at least partly driven by a centralization of effects among interhemispheric connections (see Supplementary Result 10).

Third, rich club connections are found to display significantly higher cross-disorder involvement as compared to connections of peripheral regions (Figure 3). This observation is in line with studies showing the involvement of the rich club in several disorders, such as schizophrenia [25], autism spectrum disorder [26], Huntington's disease [27], and Alzheimer's disease [17] and studies reporting on widespread overlap in gray matter and resting-state functional abnormalities across disorders in central hub regions [7]. We conclude from this that connections central to global integration of information display an elevated vulnerability across a wide range of mental disorders.

The observed cross-disorder involvement of central connections is argued to result from an accumulation of different disease mechanisms across disorders [28]. A potential heterogeneous etiology of the vulnerability of central connections is in line with the interpretation that our results

reflect small to medium effect sizes [29] and is supported by the observation that central connections are involved in both psychiatric and neurological disorders, but with different impact (Supplementary Figure 6). Several biological mechanisms and disease pathways have been proposed to contribute to this general vulnerability of central connections. Central regions and connections have been argued to be biologically expensive, characterized by complex cytoarchitecture [30], high metabolism [19] and high neuronal activity [31]. This high biological cost has been argued to cause a general vulnerability to a wide range of disease processes, such as reductions in the supply of oxygen or other metabolic resources [32]. Central connections may also display a high cross-disorder involvement as the result of their topological centrality and associated risk to propagating disease processes [28]. Furthermore, long-range central connections may be particularly vulnerable to focal white matter degeneration, with the chance of a connection being affected by random white matter lesions being proportional to its physical length, resulting in a higher predisposition of long-range central connections to general white matter atrophy compared with short range connections. Central connections of the brain have been noted to display a prolonged development [33], which may further increase their general vulnerability with these connections at elevated risk to late neurodevelopmental stress, substance use and/or dysregulation of for example hypothalamic-pituitary-adrenal axis function [34]. Alternatively, a high vulnerability of central connections might also relate to overlap in symptomatology across disorders. We observed that connections with high cross-disorder involvement connect regions involved in attention and cognitive control, which are cognitive brain functions commonly affected in a wide range of brain disorders [35].

This cross-disorder connectome study complements previous meta-analyses that localized cross-disorder vulnerability in other brain modalities such as functional hypo- and hyperactivation and gray matter abnormalities [36]. In line with our observed vulnerability of central connections, cross-disorder abnormalities in resting-state functional connectivity have been reported in brain regions important for neural integration [37]. Meta-analyses have further associated hyperconnectivity between the default mode network and executive networks with transdiagnostic factors [38], results that overlap with the here observed cross-disorder vulnerability of white matter tracts involved in cognitive control.

Integrating cross-disorder findings from multiple modalities provides the opportunity to gain further insight in the biological mechanisms that overlap and dissociate across disorders [39]. An exploratory comparison of the overlap and dissociation between previously reported [7] gray matter effects and white matter disease involvement revealed the left caudal middle frontal, left superior frontal and

left cuneus to show high cross-disorder involvement in both white-matter disconnectivity as well as gray matter abnormalities (Figure 6, see Supplementary Result 11). In contrast, regions like the left superior frontal, right paracentral, right superior frontal and right medial orbitofrontal cortex tend to show high white matter cross-disorder disconnectivity, but low general vulnerability to gray matter abnormalities, while the left fusiform area and left caudal anterior cingulate cortex tend to show high gray matter vulnerability but low cross-disorder disconnectivity involvement. The differential involvement of brain regions in both types of cross-disorder involvement suggests a complex interaction between gray and white matter cross-disorder disease pathways. Further investigation of cross-disorder mechanisms that are associated with either gray or white matter abnormalities provides a promising avenue to identify explicit cross-disorder disease pathways that are linked with specific brain phenotype outcomes.

Genetics and heritability studies offer the potential to gain further understanding of the pathology underlying cross-disorder disconnectivity. Shared genetic etiology is observed across many psychiatric and neurological disorders [40], with shared genetic risk factors providing converging evidence for common underlying biological processes across brain disorders [41]. Examination of structural disconnectivity and genetic information in a multi-modal and cross-disorder approach may further identify cross-disorder and disorder-specific biological pathways [42].

The observation of overlapping disconnectivity patterns across brain disorders is in agreement with the hypothesis that brain disorders are interrelated [41] and prompts a careful consideration of disease disconnectivity findings. Disconnectivity findings of single-disorder connectome examinations are often interpreted as disorder-specific disconnectivity effects. Such misattribution is perhaps most problematic in the development of biomarkers for brain disorders based on disconnectivity fingerprints, where it could result in overestimation of the disorder specificity of a presented biomarker. Our findings argue for a cross-disorder approach to connectome disease studies, and specifically the development of biomarkers that can disentangle disorder-shared and disorder-specific disconnectivity effects.

Several methodological issues have to be considered when interpreting our findings. While combining data from multiple studies may implicitly account for real-world heterogeneity and improve generalizability of observed results [43], it overlooks disorder-age interactions and it reduces statistical power as a result of inter-study heterogeneity in diagnoses, demographics, scanner and MRI acquisition protocols. We are aware of this limitation and aimed to match for age effects and

maximize statistical power by directly comparing patients and matched controls within each study first, before combining information across the twelve disorders. Second, disorder disconnectivity fingerprints were based on structural brain networks obtained by diffusion-based MRI, with white matter microstructural integrity assessed by means of the metric of fractional anisotropy [44]. Fractional anisotropy is however only an indirect marker of the micro-scale architecture of white matter tissue. Diffusion weighted imaging has recognized limitations with respect to the reconstruction of complex fibers and connectome mapping [45], which might result in underestimation of disconnectivity effects within and across disorders. Third, our conclusions are based on effects observed across twelve disorders, and it remains unclear whether our conclusions could be generalized to an even wider range of brain disorders. To verify that the results were not driven by a single disorder, we performed a leave-one-disorder-out validation analysis in which all analyses were repeated leaving out one disorder at a time. Moreover, we repeated all analyses using a strict set of brain disorders, excluding MCI and obesity, which showed similar results (see Supplementary Result 12). We also examined neurological and psychiatric disorders separately, confirming vulnerability of central connections in both classes of disorders. Investigating potential further clustering of disorders within these two large classes of disorders based on disorder disconnectivity patterns may provide further insights in more detailed biological relationships between and across disorders.

Our cross-disorder comparative findings suggest shared connectome pathology across brain disorders, with central connections important for global communication and neural integration forming potential 'hot spots of disconnectivity' in the human brain. Our cross-disorder comparison showed varying involvement of central connections across disorders, suggesting that each disorder may include a balance between disorder-specific and disorder-shared disconnectivity. Future examinations untangling disconnectivity effects will provide better understanding of which brain alterations are general and which effects are unique for brain disorders, providing opportunities to develop MRI based biomarkers for mental disorders.

Methods

Studies and subjects

Diffusion MRI data of 2,681 patients and controls of twelve disorders were included. All participants or legal tutors (in case of children under the age of 18) provided written informed consent and all studies were approved by their local ethics committee for research in humans (see Supplementary Method 1). Data included diffusion-weighted imaging (DWI) data of previously reported studies on

schizophrenia (three datasets available, set I, II and III) (COBRE, [46] and [47]), bipolar disorder [48], attention deficit hyperactivity disorder (ADHD) [49], autism spectrum disorder (ASD, four datasets) (ABIDEII and the study of van Belle et al. [49]), major depressive disorder (MDD) [50], obesity [51], obsessive-compulsive disorder (OCD) [52], posttraumatic stress disorder (PTSD, two datasets, set I and set II) (ADNI-DOD adni.loni.usc.edu and [53]), and four neurological disorders, Alzheimer's disease (AD, two datasets, set I and set II) (ADNI and [54]), mild cognitive impairment (MCI, two datasets, set I and set II) (ADNI and [54]), amyotrophic lateral sclerosis (ALS) [55] and primary lateral sclerosis (PLS) [55]). Supplementary Figure 1 provides an overview of all data included and a summary is provided in Table 1. Further details including MRI acquisition protocols and demographics are outlined in Supplementary Method 1 and Supplementary Table 2. Within each dataset, patients and controls were matched on age, sex, scanner settings and where possible other demographics (procedure described in the Supplementary Method 2).

Data processing

DWI Tractography. Data preprocessing of DWI and T1-weighted images of individuals included the following steps: the anatomical T1-weighted image was parcellated into 219 distinct cortical regions (111 left-hemispheric and 108 right-hemispheric regions) according to a subdivision of FreeSurfer's Desikan-Killiany atlas [56] using FreeSurfer [57]. This subdivision provided high methodological robustness while remaining sensitive to changes in connectivity [56]. Underscoring the influence of parcellation and network size on network measures [58], we repeated analyses using a different subparcellation of the Desikan-Killiany atlas (DK-114, 114 regions, data presented in the variation analyses section and Supplementary Result 1). Second, the individual parcellation map was co-registered to the DWI data using an affine transformation mapping of the T1-weighted image to the DWI image. Third, diffusion-weighted images were corrected for eddy current distortions and head motion using the FMRIB Software Library [59]. If reversed phase encoding data was available (datasets listed in SI Table 2), susceptibility induced distortions were estimated and incorporated in the preprocessing [60]. Fourth, a tensor was fitted to the diffusion signals in each voxel using a robust tensor fitting algorithm [61] and subsequently fractional anisotropy (FA) was derived [62]. Given the mostly clinical diffusion MRI protocols used for data acquisition, simple deterministic tensor reconstruction (DTI) (as compared to more advanced diffusion profile reconstruction methods) was used to minimize the potential influence of false positives on network reconstruction and subsequent computation of network metrics [15]. This relatively simple reconstruction of the diffusion signal is a limitation of our cross-disorder examination, potentially leading to incomplete reconstruction of complex fiber pathways and an underestimation of cross-disorder disease effects [63]. Fifth, white matter pathways were reconstructed using fiber assignment by continuous tracking

(FACT) [64], with streamline reconstruction starting from eight seeds in every cerebral white matter voxel. Fiber tracking was continued until a streamline showed high curvature (> 45º), exited the brain mask, or when a streamline entered a voxel with low fractional anisotropy (< 0.1). The mean FA value of a streamline was computed as the weighted average FA value over all voxels that a streamline passed.

Network reconstruction. For each individual dataset, reconstructed streamlines and cortical parcellation were combined into a weighted network. The 219 cortical areas were chosen as nodes in the network and two regions were considered connected if at least one reconstructed streamline was found to touch both cortical regions. The weight of connections was taken as the mean fractional anisotropy (FA) of streamlines involved [44]. An overview of FA distribution per dataset and patient and control group is provided in Supplementary Figure 12 and Supplementary Table 3.

Cross-disorder analysis

Cross-disorder examination of disorder-related disconnectivity was performed in two steps. Patient and control data were first compared within each dataset (in contrast to the alternative of pooling all data into one large dataset) to ensure that patients and controls were matched on age, sex and other demographics and scanner settings. This comparison provided for each disorder a disconnectivity map quantifying the differences in connectivity strength between patients and matched controls. Second, patient-control matched disorder disconnectivity maps were combined across the twelve disorders to determine the distribution of disconnectivity effects across network connections of the brain. This two-step approach optimized comparability of data across studies with different MRI acquisition protocols. In what follows, we describe this procedure in more detail, including the construction of the disorder disconnectivity maps and the cross-disorder involvement map, followed by the performed statistical analyses.

Step 1: Disorder disconnectivity map

Per disorder, a disconnectivity map was constructed by assessing the between-group difference in FA of connections between patients and controls quantified by a Student's t-test statistic. As such, we tested for lowered FA connectivity strength in the patient group compared to the controls. To incorporate possible differences in degrees of freedom across connections, t-test statistics were transformed to z-scores derived from the p-values using the equivalent area under the curve.
For the disorders ASD, PTSD, schizophrenia, Alzheimer's disease and MCI, for which multiple datasets were available, a disorder disconnectivity map was calculated per dataset and then combined into an average disorder disconnectivity map using Stouffer's method for combining

independent tests by averaging the z-scores in the disorder disconnectivity maps across datasets weighted proportional to the effective sample size of the dataset [65].

In total, this resulted in a disorder disconnectivity map for each of the 12 included brain disorders. Next, the top 15% connections with highest z-scores were selected as the set of most involved connections in that disorder, performing, per disorder, a proportional thresholding on the disorder-specific disconnectivity map with a density of 15% [66]. Results using 5%, 10%, 20% or 25% involved connections are presented in the Supplementary Result 2. Results using a second selection-free meta-analysis method in which connection involvement was weighted by the full z-scores in the disorder disconnectivity maps are also presented in the Supplementary Result 3.

Step 2: Cross-disorder involvement map

The twelve thresholded and patient-control matched disorder disconnectivity maps were combined into a total cross-disorder involvement map. To maximize comparability across studies and to avoid any potential bias to one of the included datasets, connection effects were included for those connections present in a reference connectome map based on high-quality data of the Human Connectome Project (HCP, 500 Subjects Release of the Human Connectome Project) [67] (see Supplementary Method 3 for details on the HCP group connectome reconstruction). A cross-disorder involvement map was formed by adding up all thresholded disorder disconnectivity maps and dividing it by the number of disorders in which each connection was present, thus computing per connection the percentage of disorders in which this connection was involved.

White matter bundles

The Johns Hopkins University ICBM-DTI-81 white-matter atlas as included in FSL was used as a segmentation of 48 white matter bundles in standard MNI space [68]. The extent to which each reconstructed connection overlapped with a bundle was computed as a percentage of overlap based on high-resolution tractography of subjects in the reference connectome dataset. The volume (i.e. number of voxels) shared between a connection and bundle was computed, divided by the total volume of the bundle in each subject and averaged across subjects, providing the percentage of overlap between a connection and bundle. Cross-disorder involvement of white-matter bundles was then calculated as the sum of cross-disorder involvement over all connections weighted by this percentage of overlap. Ten bundles showed no overlap with any of the reconstructed connections and were excluded from the analysis (See Supplementary Table 4 for an overview of the 38 included white matter bundles). This procedure was repeated for the 10,000 randomized cross-disorder involvement maps, providing for each white matter bundle a null-model of cross-disorder

involvement under subject-label permutation. Significance was assessed using permutation testing (Bonferroni correction was applied to correct for multiple testing across 38 white matter bundles).

Region-wise cross-disorder involvement

Region-wise cross-disorder involvement was derived by averaging cross-disorder involvement of connections adjacent to each region. Functional correlates of high regional cross-disorder involvement were examined using brain function maps obtained from the NeuroSynth database (www.neurosynth.org) [69]. The NeuroSynth database provides statistical mapping in standard MNI space of neural and cognitive states, named "terms", based on a meta-analysis of literature. For every term, we downloaded the association-test map that displays the preferential association of voxels with the term. A regional term involvement map was formed by combining the association-test statistics across all voxels of each brain region using sample size based meta-analysis [70]. We examined 24 groupings of 99 terms that described distinct interpretable brain functions [71]. The associated regional brain function involvement maps were computed as the number of terms per brain function that exceeded a z-score threshold of 2.6 in a region. Next, the region-wise cross-disorder involvement map was correlated with all regional topic maps to identify which topics had similar regional distributions as the cross-disorder involvement map (normality of the data distributions was not formally tested and Bonferroni correction was applied to correct for multiple testing across 24 functions).

Network analysis

The centrality of connections in the network structure was considered with respect to rich club organization, edge-wise global and local network measures and physical wiring length. Metrics were computed on the reference connectome to ensure independence of the examined datasets.

Global network organization. Global network integration was examined from the perspective of the ease of communication between nodes in the network. Centrality of connections with respect to the shortest topological paths in the network was measured by counting the number of shortest topological paths through each network connection using the metric of edge betweenness [72]. Network integration was considered by examining the metric of network communicability, measuring all possible walks between nodes [11]. The contribution of connections to communicability was assessed by edge-removal statistics [73]. Removal-effect of each connection on network communicability was quantified as the difference (in terms of percentage) between the network communicability before and after removal of a connection.

Local network organization. The role of network connections in local network organization was assessed through the contribution of each connection to network clustering [72]. The removal-effect of each connection on global network clustering was quantified as the difference (i.e., percentage of change) in global clustering before and after removal of the connection.

Spatial embedding. Projection length of each connection was calculated as the average physical length of a connection in the HCP reference dataset.

Rich club organization. Central connections were identified with respect to the rich club organization of the reference network, describing the total collective of high-degree hub regions and their connections [12]. Regional degree was computed on the basis of the reference connectome to avoid any potential data-driven bias in any class of connections towards the included datasets. Hub regions were selected as regions with a degree above 14 (top 13% regions with the highest regional degree, 29 regions, Supplementary Figure 4, listed in Supplementary Table 5) in line with previous hub definitions [2]. Network connections were subsequently categorized into rich club connections, describing connections spanning between hub regions, feeder connections, describing connections spanning between hub and peripheral regions, or local connections, describing connections between peripheral regions [2]. Analyses were repeated with connections classes derived from a smaller and larger set of hub regions, revealing consistent results (see Supplementary Result 6).

Statistical analysis

Cross-disorder involvement. Significant subnetworks in the brain with increased cross-disorder involvement levels were identified using Network Based Statistics [9]. The cross-disorder involvement map was binarized by including connections with cross-disorder involvement percentages above a specified NBS-threshold. Multiple NBS-thresholds (0%, 5%, …, 100%) were considered, capturing the trade-off between specificity and sensitivity of the NBS-analysis. The number of connections in the greatest component of the thresholded network was counted. Significance of this cluster was assessed using permutation testing by comparison with the distribution of greatest component sizes in a null condition in which disease effects were randomized. For this, for each permutation, a cross-disorder involvement map was calculated on a permuted subject sample in which subject labels (i.e. controls and patients) were randomly reassigned (keeping patient and control group sizes intact). 10,000 permutations were examined and the percentage of the permutations in which the greatest component was larger or equal to the observed greatest component was assigned as p-value to the observed cross-disorder involvement. We used an alpha level of 0.05 for this and all other tests.

Edge-wise centrality measures. The 25% most central connections selected by global network integration, local network integration and the spatial embedding were examined. In the variation

analyses, also other reasonable percentages (5%, 10%, …, 45%) for selecting central connections were examined and verified to show similar results. Cross-disorder involvement levels were compared with the levels expected when disconnectivity was randomly distributed using permutation testing, this to verify independence of our results from connection properties such as connection prevalence or group-average connection strength. For each permutation, subject labels were randomly reassigned and cross-disorder involvement maps were calculated using the permuted subject-labeling. 10,000 permutations were computed and cross-disorder involvement levels of the subsets of central connections were calculated for each permutation. Based on this null distribution, the original effect was assigned a p-value as the percentage of permutations in which the cross-disorder involvement was equal to or exceeded the observed cross-disorder involvement. Standardized effect sizes were measured by Cohen's d approximated as difference between the observed average cross-disorder involvement of central connections and the average cross-disorder involvement of central connections in subject-label permuted cross-disorder involvement maps divided by the standard deviation of the observed cross-disorder involvement of central connections.

Rich club organization. Differences in mean cross-disorder involvement between rich club and feeder, rich club and local, and feeder and local connection classes were statistically assessed using permutation testing (10,000 permutations). In each permutation, connection class labels were randomly shuffled and mean cross-disorder involvement of the classes was computed over the permuted connections. Differences in cross-disorder involvement between connection classes were computed for all permutations. The observed difference in cross-disorder involvement between two connection classes was assigned a p-value by computing the percentage of permutations in which the difference between the two connection classes was equal to or exceeded the observed difference. Standardized effect sizes were approximated using Cohen's d calculated as the difference between average cross-disorder involvement of two connection classes divided by the pooled standard deviation.

Global white matter

Additional permutation testing was performed to verify independence of our results from widespread white matter differences in fractional anisotropy. For each subject, global FA was computed as the total FA strength of all connections. Next, subjects were classified into ten global FA groups, group one with global FA in the interval [0, 0.1), group two with global FA in the interval [0.1, 0.2), etc. For permutation testing, subject labels were permuted within datasets, but now under the constraint of only allowing switching patient and control labels of subjects assigned to the

same global FA bin. As such, the resulting global FA distribution of permuted patient and control groups was kept similar to the original global FA distributions (and therewith also potential between-group differences in global FA). 10,000 permutations were computed and, in each permutation, the cross-disorder involvement of the subsets of connections was calculated. Observed effects were assigned a p-value as the percentage of the permutations in which the measured effect was equal to or exceeded the observed effect.

Data availability

The reference connectome dataset was based on data from the Human Connectome Project which is available from https://www.humanconnectome.org

Datasets ASD II, ASD III and ASD IV were obtained from the ABIDE-II database and are available from http://fcon_1000.projects.nitrc.org/indi/abide/abide_II.html

Datasets Alzheimer's disease II, MCI II and PTSD II were obtained from the ADNI and DOD-ADNI database and are available from http://adni.loni.usc.edu

Dataset Schizophrenia III was obtained from the COBRE database and is available from http://fcon_1000.projects.nitrc.org/indi/retro/cobre.html

Datasets ADHD I, ALS, Alzheimer's disease I, ASD I, Bipolar disorder, MCI I, MDD, Obesity, OCD, PLS, PTSD I, Schizophrenia I and Schizophrenia II are subject to specific data-sharing restrictions. To inquire about access to the restricted datasets, please get in touch with the corresponding author.

Code availability

All code is available from the corresponding author upon reasonable request.

References

1 Bullmore, E. & Sporns, O. The economy of brain network organization. *Nature Reviews Neuroscience* **13**, 336-336, doi:10.1038/nrn3214 (2012).

2 van den Heuvel, M. P., Kahn, R. S., Goñi, J. & Sporns, O. High-cost, high-capacity backbone for global brain communication. *Proceedings of the National Academy of Sciences of the United States of America* **109**, 11372-11377, doi:10.1073/pnas.1203593109 (2012).

3 Baggio, H. C. *et al.* Rich Club Organization and Cognitive Performance in Healthy Older Participants. *Journal of Cognitive Neuroscience* **27**, 1801-1810, doi:10.1162/jocn_a_00821 (2015).

4 Goodkind, M. *et al.* Identification of a common neurobiological substrate for mental illness. *JAMA psychiatry* **72**, 305-315, doi:10.1001/jamapsychiatry.2014.2206 (2015).
5 Brainstorm, C. *et al.* Analysis of shared heritability in common disorders of the brain. *Science* **360**, doi:10.1126/science.aap8757 (2018).
6 Nuyen, J. *et al.* Comorbidity was associated with neurologic and psychiatric diseases: A general practice-based controlled study. *Journal of Clinical Epidemiology* **59**, 1274-1284, doi:10.1016/j.jclinepi.2006.01.005 (2006).
7 Crossley, N. A. *et al.* The hubs of the human connectome are generally implicated in the anatomy of brain disorders. *Brain* **137**, 2382-2395, doi:10.1093/brain/awu132 (2014).
8 Fornito, A. & Bullmore, E. T. Connectomics: A new paradigm for understanding brain disease. *European Neuropsychopharmacology* **25**, 733-748, doi:10.1016/j.euroneuro.2014.02.011 (2015).
9 Zalesky, A., Fornito, A. & Bullmore, E. T. Network-based statistic: Identifying differences in brain networks. *NeuroImage* **53**, 1197-1207, doi:10.1016/j.neuroimage.2010.06.041 (2010).
10 Glasser, M. F. *et al.* The minimal preprocessing pipelines for the Human Connectome Project. *NeuroImage* **80**, 105-124, doi:10.1016/j.neuroimage.2013.04.127 (2013).
11 Estrada, E. & Hatano, N. Communicability in complex networks. *Physical Review E* **77**, 036111-036111, doi:10.1103/PhysRevE.77.036111 (2008).
12 van den Heuvel, M. P. & Sporns, O. Rich-Club Organization of the Human Connectome. *The Journal of Neuroscience* **31**, 15775-15786, doi:10.1523/jneurosci.3539-11.2011 (2011).
13 van den Heuvel, M. P., Bullmore, E. T. & Sporns, O. Comparative Connectomics. *Trends in cognitive sciences* **20**, 345-361, doi:10.1016/j.tics.2016.03.001 (2016).
14 Ellison-Wright, I. & Bullmore, E. Meta-analysis of diffusion tensor imaging studies in schizophrenia. *Schizophrenia Research* **108**, 3-10, doi:10.1016/j.schres.2008.11.021 (2009).
15 de Reus, M. A. & van den Heuvel, M. P. Estimating false positives and negatives in brain networks. *NeuroImage* **70**, 402-409, doi:10.1016/j.neuroimage.2012.12.066 (2013).
16 Betzel, R. F., Griffa, A., Hagmann, P. & Mišić, B. Distance-dependent consensus thresholds for generating group-representative structural brain networks. *Network Neuroscience*, 1-22, doi:10.1162/netn_a_00075 (2018).
17 Bai, F. *et al.* Topologically Convergent and Divergent Structural Connectivity Patterns between Patients with Remitted Geriatric Depression and Amnestic Mild Cognitive Impairment. *Journal of Neuroscience* **32** (2012).
18 Griffa, A., Baumann, P. S., Thiran, J.-P. & Hagmann, P. Structural connectomics in brain diseases. *NeuroImage* **80**, 515-526, doi:10.1016/j.neuroimage.2013.04.056 (2013).

19 Bullmore, E. T. & Sporns, O. The economy of brain network organization. *Nature reviews. Neuroscience* **13**, 336-349, doi:10.1038/nrn3214 (2012).

20 Griffa, A. & van den Heuvel, M. P. Rich-club neurocircuitry: function, evolution, and vulnerability. *Dialogues in clinical neuroscience* **20**, 121-132 (2018).

21 Hamilton, L. S. *et al.* Reduced white matter integrity in attention-deficit hyperactivity disorder. *Neuroreport* **19**, 1705-1708, doi:10.1097/WNR.0b013e3283174415 (2008).

22 Koldewyn, K. *et al.* Differences in the right inferior longitudinal fasciculus but no general disruption of white matter tracts in children with autism spectrum disorder. *Proceedings of the National Academy of Sciences of the United States of America* **111**, 1981-1986, doi:10.1073/pnas.1324037111 (2014).

23 Peng, Z. *et al.* Brain structural abnormalities in obsessive-compulsive disorder: Converging evidence from white matter and grey matter. *Asian Journal of Psychiatry* **5**, 290-296, doi:10.1016/J.AJP.2012.07.004 (2012).

24 Ashtari, M. *et al.* Disruption of White Matter Integrity in the Inferior Longitudinal Fasciculus in Adolescents With Schizophrenia as Revealed by Fiber Tractography. *Archives of General Psychiatry* **64**, 1270-1270, doi:10.1001/archpsyc.64.11.1270 (2007).

25 van den Heuvel, M. P. *et al.* Abnormal Rich Club Organization and Functional Brain Dynamics in Schizophrenia. *JAMA Psychiatry* **70**, 783-783, doi:10.1001/jamapsychiatry.2013.1328 (2013).

26 Grayson, D. S. *et al.* Structural and functional rich club organization of the brain in children and adults. *PloS one* **9**, e88297-e88297, doi:10.1371/journal.pone.0088297 (2014).

27 McColgan, P. *et al.* Selective vulnerability of Rich Club brain regions is an organizational principle of structural connectivity loss in Huntington's disease. *Brain* **138**, 3327-3344, doi:10.1093/brain/awv259 (2015).

28 Fornito, A., Zalesky, A. & Breakspear, M. The connectomics of brain disorders. *Nature Reviews Neuroscience* **16**, 159-172, doi:10.1038/nrn3901 (2015).

29 Paulus, M. P. & Thompson, W. K. The Challenges and Opportunities of Small Effects. *JAMA Psychiatry*, doi:10.1001/jamapsychiatry.2018.4540 (2019).

30 van den Heuvel, M. P., Scholtens, L. H., Feldman Barrett, L., Hilgetag, C. C. & de Reus, M. A. Bridging Cytoarchitectonics and Connectomics in Human Cerebral Cortex. *Journal of Neuroscience* **35**, 13943-13948, doi:10.1523/JNEUROSCI.2630-15.2015 (2015).

31 de Haan, W., Mott, K., van Straaten, E. C. W., Scheltens, P. & Stam, C. J. Activity Dependent Degeneration Explains Hub Vulnerability in Alzheimer's Disease. *PLoS Computational Biology* **8**, e1002582-e1002582, doi:10.1371/journal.pcbi.1002582 (2012).

32 Buckner, R. L. *et al.* Cortical hubs revealed by intrinsic functional connectivity: mapping, assessment of stability, and relation to Alzheimer's disease. *J Neurosci* **29**, 1860-1873, doi:10.1523/JNEUROSCI.5062-08.2009 (2009).
33 Baker, S. T. E. *et al.* Developmental Changes in Brain Network Hub Connectivity in Late Adolescence. *The Journal of neuroscience : the official journal of the Society for Neuroscience* **35**, 9078-9087, doi:10.1523/JNEUROSCI.5043-14.2015 (2015).
34 Dennis, E. L. *et al.* Development of the “rich club” in brain connectivity Networks from 438 adolescents & adults aged 12 to 30. *Proceedings. IEEE International Symposium on Biomedical Imaging*, 624-627, doi:10.1109/ISBI.2013.6556552 (2013).
35 McTeague, L. M. *et al.* Identification of Common Neural Circuit Disruptions in Cognitive Control Across Psychiatric Disorders. *American Journal of Psychiatry* **174**, 676-685, doi:10.1176/appi.ajp.2017.16040400 (2017).
36 Sprooten, E. *et al.* Addressing reverse inference in psychiatric neuroimaging: Meta-analyses of task-related brain activation in common mental disorders. *Human Brain Mapping*, doi:10.1002/hbm.23486 (2016).
37 Sha, Z. *et al.* Meta-Connectomic Analysis Reveals Commonly Disrupted Functional Architectures in Network Modules and Connectors across Brain Disorders. *Cerebral Cortex* **28**, 4179-4194, doi:10.1093/cercor/bhx273 (2018).
38 Elliott, M. L., Romer, A., Knodt, A. R. & Hariri, A. R. A Connectome-wide Functional Signature of Transdiagnostic Risk for Mental Illness. *Biological Psychiatry* **84**, 452-459, doi:10.1016/j.biopsych.2018.03.012 (2018).
39 Cauda, F. *et al.* Brain structural alterations are distributed following functional, anatomic and genetic connectivity. *Brain* **141**, 3211-3232, doi:10.1093/brain/awy252 (2018).
40 Cross-Disorder Group of the Psychiatric Genomics Consortium, C.-D. G. o. t. P. G. *et al.* Genetic relationship between five psychiatric disorders estimated from genome-wide SNPs. *Nature genetics* **45**, 984-994, doi:10.1038/ng.2711 (2013).
41 Doherty, J. L. & Owen, M. J. Genomic insights into the overlap between psychiatric disorders: implications for research and clinical practice. *Genome medicine* **6**, 29-29, doi:10.1186/gm546 (2014).
42 Lee, P. H. *et al.* Partitioning heritability analysis reveals a shared genetic basis of brain anatomy and schizophrenia. *Molecular psychiatry* **21**, 1680-1689, doi:10.1038/mp.2016.164 (2016).
43 Sweeney, T. E., Haynes, W. A., Vallania, F., Ioannidis, J. P. & Khatri, P. Methods to increase reproducibility in differential gene expression via meta-analysis. *Nucleic acids research* **45**, e1-e1, doi:10.1093/nar/gkw797 (2017).

44 Beaulieu, C. The basis of anisotropic water diffusion in the nervous system - a technical review. *NMR in Biomedicine* **15**, 435-455, doi:10.1002/nbm.782 (2002).
45 van den Heuvel, M. P. *et al.* Comparison of diffusion tractography and tract-tracing measures of connectivity strength in rhesus macaque connectome. *Human Brain Mapping* **36**, 3064-3075, doi:10.1002/hbm.22828 (2015).
46 Collin, G., Kahn, R. S., de Reus, M. A., Cahn, W. & van den Heuvel, M. P. Impaired Rich Club Connectivity in Unaffected Siblings of Schizophrenia Patients. *Schizophrenia Bulletin* **40**, 438-448, doi:10.1093/schbul/sbt162 (2014).
47 Svatkova, A. *et al.* Physical Exercise Keeps the Brain Connected: Biking Increases White Matter Integrity in Patients With Schizophrenia and Healthy Controls. *Schizophrenia bulletin* **41**, 869-878, doi:10.1093/schbul/sbv033 (2015).
48 Collin, G. *et al.* Brain network analysis reveals affected connectome structure in bipolar I disorder. *Human Brain Mapping* **37**, 122-134, doi:10.1002/hbm.23017 (2016).
49 van Belle, J., van Hulst, B. M. & Durston, S. Developmental differences in intra-individual variability in children with ADHD and ASD. *Journal of Child Psychology and Psychiatry* **56**, 1316-1326, doi:10.1111/jcpp.12417 (2015).
50 Repple, J. *et al.* A voxel-based diffusion tensor imaging study in unipolar and bipolar depression. *Bipolar Disorders* **19**, 23-31, doi:10.1111/bdi.12465 (2017).
51 Marqués-Iturria, I. *et al.* Affected connectivity organization of the reward system structure in obesity. *NeuroImage* **111**, 100-106, doi:10.1016/j.neuroimage.2015.02.012 (2015).
52 Reess, T. J. *et al.* Connectomics-based structural network alterations in obsessive-compulsive disorder. *Translational Psychiatry* **6**, e882-e882, doi:10.1038/tp.2016.163 (2016).
53 Kennis, M. *et al.* Treatment Outcome-Related White Matter Differences in Veterans with Posttraumatic Stress Disorder. *Neuropsychopharmacology : official publication of the American College of Neuropsychopharmacology* **40**, 2434-2442, doi:10.1038/npp.2015.94 (2015).
54 Serra, L. *et al.* Network-Based Substrate of Cognitive Reserve in Alzheimer's Disease. *Journal of Alzheimer's Disease* **55**, 421-430, doi:10.3233/JAD-160735 (2016).
55 van der Burgh, H. K. *et al.* Deep learning predictions of survival based on MRI in amyotrophic lateral sclerosis. *NeuroImage: Clinical*, doi:10.1016/j.nicl.2016.10.008 (2016).
56 Cammoun, L. *et al.* Mapping the human connectome at multiple scales with diffusion spectrum MRI. *Journal of Neuroscience Methods* **203**, 386-397, doi:10.1016/j.jneumeth.2011.09.031 (2012).
57 Fischl, B. *et al.* Automatically Parcellating the Human Cerebral Cortex. *Cerebral Cortex* **14**, 11-22, doi:10.1093/cercor/bhg087 (2004).

58 Zalesky, A. *et al.* Whole-brain anatomical networks: Does the choice of nodes matter? *NeuroImage* **50**, 970-983, doi:10.1016/J.NEUROIMAGE.2009.12.027 (2010).

59 Andersson, J. L. R. & Sotiropoulos, S. N. An integrated approach to correction for off-resonance effects and subject movement in diffusion MR imaging. *NeuroImage* **125**, 1063-1078, doi:10.1016/j.neuroimage.2015.10.019 (2016).

60 Andersson, J. L. R., Skare, S. & Ashburner, J. How to correct susceptibility distortions in spin-echo echo-planar images: Application to diffusion tensor imaging. *NeuroImage* **20**, 870-888, doi:10.1016/S1053-8119(03)00336-7 (2003).

61 Chang, L. C., Walker, L. & Pierpaoli, C. Informed RESTORE: A method for robust estimation of diffusion tensor from low redundancy datasets in the presence of physiological noise artifacts. *Magnetic Resonance in Medicine* **68**, 1654-1663, doi:10.1002/mrm.24173 (2012).

62 Alexander, A. L., Lee, J. E., Lazar, M. & Field, A. S. Diffusion tensor imaging of the brain. *Neurotherapeutics : the journal of the American Society for Experimental NeuroTherapeutics* **4**, 316-329, doi:10.1016/j.nurt.2007.05.011 (2007).

63 Maier-Hein, K. H. *et al.* The challenge of mapping the human connectome based on diffusion tractography. *Nature Communications* **8**, 1349-1349, doi:10.1038/s41467-017-01285-x (2017).

64 Mori, S., Crain, B. J., Chacko, V. P. & van Zijl, P. C. M. Three-dimensional tracking of axonal projections in the brain by magnetic resonance imaging. *Annals of Neurology* **45**, 265-269, doi:10.1016/j.echo.2007.08.009 (1999).

65 Riley, J. W. *et al.* The American Soldier: Adjustment During Army Life. *American Sociological Review* **14**, 557-557 (1949).

66 van den Heuvel, M. *et al.* Proportional thresholding in resting-state fMRI functional connectivity networks and consequences for patient-control connectome studies: Issues and recommendations. *NeuroImage*, doi:10.1016/j.neuroimage.2017.02.005 (2017).

67 Van Essen, D. C. *et al.* The Human Connectome Project: a data acquisition perspective. *NeuroImage* **62**, 2222-2231, doi:10.1016/j.neuroimage.2012.02.018 (2012).

68 Mori, S. *et al.* Stereotaxic white matter atlas based on diffusion tensor imaging in an ICBM template. *NeuroImage* **40**, 570-582, doi:10.1016/J.NEUROIMAGE.2007.12.035 (2008).

69 Yarkoni, T., Poldrack, R. A., Nichols, T. E., Van Essen, D. C. & Wager, T. D. Large-scale automated synthesis of human functional neuroimaging data. *Nature Methods* **8**, 665-670, doi:10.1038/nmeth.1635 (2011).

70 Willer, C. J., Li, Y. & Abecasis, G. R. METAL: fast and efficient meta-analysis of genomewide association scans. *Bioinformatics (Oxford, England)* **26**, 2190-2191, doi:10.1093/bioinformatics/btq340 (2010).

71 Margulies, D. S. *et al.* Situating the default-mode network along a principal gradient of macroscale cortical organization. *Proceedings of the National Academy of Sciences of the United States of America* **113**, 12574-12579, doi:10.1073/pnas.1608282113 (2016).
72 Rubinov, M. & Sporns, O. Complex network measures of brain connectivity: uses and interpretations. *NeuroImage* **52**, 1059-1069, doi:10.1016/j.neuroimage.2009.10.003 (2010).
73 Irimia, A. & Van Horn, J. D. Systematic network lesioning reveals the core white matter scaffold of the human brain. *Frontiers in Human Neuroscience* **8**, 51-51, doi:10.3389/fnhum.2014.00051 (2014).
74 Schmidt, R. *et al.* Correlation between structural and functional connectivity impairment in amyotrophic lateral sclerosis. *Human brain mapping* **35**, 4386-4395, doi:10.1002/hbm.22481 (2014).
75 Mancini, M. *et al.* Network attack simulations in Alzheimer's disease: The link between network tolerance and neurodegeneration. 237-240, doi:10.1109/ISBI.2016.7493253.

Acknowledgements

M.P. van den Heuvel was funded by an ALW open (ALWOP.179) and VIDI (452-16-015) grant from the Netherlands Organization for Scientific Research (NWO) and a Fellowship of MQ. The Muenster Depression Cohort was funded by the German Research Foundation (DFG, grant FOR2107 DA1151/5-1 and DA1151/5-2) to UD; SFB-TRR58, Projects C09 and Z02 to UD) and the Interdisciplinary Center for Clinical Research (IZKF) of the medical faculty of Münster (grant Dan3/012/17 to UD). K. Koch was funded by the German Research Foundation (DFG, grant KO3744/7-1). N.E.M. van Haren was supported by VIDI-grant 452-11-014 from the Dutch organisation for scientific research. M.H.J. Hillegers received research support from The European Community's Health Seventh Framework Programme (grant agreement no. F2-2008-222968), NARSAD Brain and Behavior foundation (grant no. 20244) and The Netherlands Organization for Health Research and Development (MARIO grant no. 636100004). L.H. van den Berg serves on scientific advisory boards for Orion, Biogen, and Cytokinetics; received an educational grant from Baxalta; serves on the editorial boards of Amyotrophic Lateral Sclerosis and Frontotemporal Degeneration and the Journal of Neurology, Neurosurgery, and Psychiatry; and receives research support from the Prinses Beatrix Spierfonds, Netherlands ALS Foundation, The European Community's Health Seventh Framework Programme (grant agreement no. 259867), and The Netherlands Organization for Health Research and Development (Vici Scheme, JPND [SOPHIA, STRENGTH, ALSCare]). Data collection and sharing for this project was funded by the Alzheimer's

Disease Neuroimaging Initiative (ADNI) (National Institutes of Health Grant U01 AG024904) and DOD ADNI (Department of Defense award number W81XWH-12-2-0012). ADNI is funded by the National Institute on Aging, the National Institute of Biomedical Imaging and Bioengineering, and through generous contributions from the following: AbbVie, Alzheimer's Association; Alzheimer's Drug Discovery Foundation; Araclon Biotech; BioClinica, Inc.; Biogen; Bristol-Myers Squibb Company; CereSpir, Inc.; Cogstate; Eisai Inc.; Elan Pharmaceuticals, Inc.; Eli Lilly and Company; EuroImmun; F. Hoffmann-La Roche Ltd and its affiliated company Genentech, Inc.; Fujirebio; GE Healthcare; IXICO Ltd.; Janssen Alzheimer Immunotherapy Research & Development, LLC.; Johnson & Johnson Pharmaceutical Research & Development LLC.; Lumosity; Lundbeck; Merck & Co., Inc.; Meso Scale Diagnostics, LLC.; NeuroRx Research; Neurotrack Technologies; Novartis Pharmaceuticals Corporation; Pfizer Inc.; Piramal Imaging; Servier; Takeda Pharmaceutical Company; and Transition Therapeutics. The Canadian Institutes of Health Research is providing funds to support ADNI clinical sites in Canada. Private sector contributions are facilitated by the Foundation for the National Institutes of Health (www.fnih.org). The grantee organization is the Northern California Institute for Research and Education, and the study is coordinated by the Alzheimer's Therapeutic Research Institute at the University of Southern California. ADNI data are disseminated by the Laboratory for Neuro Imaging at the University of Southern California. COBRE data was downloaded from the Collaborative Informatics and Neuroimaging Suite Data Exchange tool (COINS; http://coins.mrn.org/dx) and data collection was performed at the Mind Research Network, and funded by a Center of Biomedical Research Excellence (COBRE) grant 5P20RR021938/P20GM103472 from the NIH to Dr. Vince Calhoun. Data obtained from the SchizConnect database was funded by NIMH cooperative agreement 1U01 MH097435." The database ABIDE II is primarily funded by NIMH 5R21MH107045. Data were provided in part by the Human Connectome Project, WU-Minn Consortium (Principal Investigators: David Van Essen and Kamil Ugurbil; 1U54MH091657) funded by the 16 NIH Institutes and Centers that support the NIH Blueprint for Neuroscience Research; and by the McDonnell Center for Systems Neuroscience at Washington University. The funders had no role in study design, data collection and analysis, decision to publish or preparation of the manuscript

Author contributions

M.P.H. conceived the project. S.C.L. analyzed the data. M.P.H and S.C.L. wrote the manuscript. L.H.S. provided expertise and feedback on the manuscript. L.H.B., M.P.B., M.B., W.C., U.D., S.D., E.G., N.E.M.H, M.H.J.H, K.K., M.A.J., M.M., I.M.I. S.M., R.A.O., T.J.R., J.R., R.S.K contributed data and

provided feedback on the manuscript. Data used in preparation of this article were obtained from the Alzheimer's Disease Neuroimaging Initiative (ADNI) database (adni.loni.usc.edu). As such, the investigators within the ADNI contributed to the design and implementation of ADNI and/or provided data but did not participate in analysis or writing of this report. A complete listing of ADNI investigators can be found at: http://adni.loni.usc.edu/wp-content/uploads/how_to_apply/ADNI_Acknowledgement_List.pdf

Competing interests

L.H. van den Berg serves on scientific advisory boards for Orion, Biogen, and Cytokinetics; received an educational grant from Baxalta; serves on the editorial boards of Amyotrophic Lateral Sclerosis and Frontotemporal Degeneration and the Journal of Neurology, Neurosurgery, and Psychiatry; and receives research support from the Prinses Beatrix Spierfonds, Netherlands ALS Foundation, The European Community's Health Seventh Framework Programme (grant agreement no. 259867), and The Netherlands Organization for Health Research and Development (Vici Scheme, JPND [SOPHIA, STRENGTH, ALSCare]). Other authors declare no competing interests.

Figures

Figure 1. Cross-disorder involvement. (a) Overview of data aggregation and analysis. Per disorder, a connection-wise disorder-specific disconnectivity map was computed contrasting the fractional anisotropy of connections in patients and matched controls. Disorder-specific disconnectivity maps were combined to determine the disconnectivity distribution across disorders. (b) Schematic representation of the human reference connectome with connections colored by cross-disorder involvement. (c) Superior (left panel), frontal (right-top panel) and medial (right-bottom panel) view of brain connectivity colored by cross-disorder involvement. (d) Lateral and medial view of left and right hemispheres showing region-wise cross-disorder involvement. (e) Network including 80 regions (colored blue) that showed significant involvement across disorders (NBS analysis, $p < 0.001$, one-sided permutation testing, 10,000 permutations).

Figure 2. Edge-wise network measures. From left to right, average cross-disorder involvement of connections with highest edge betweenness centrality (top 25%, n = 290, shown), contributing most to communicability, contributing most to clustering and long-distance connections. Observed values (blue) were compared with average cross-disorder involvement of central connections in subject-label permuted cross-disorder involvement maps (grey). Connections important for global topological (edge betweenness centrality: $d = 0.41$, one-sided permutation testing, 10,000 permutations, $p < 0.001$; and communicability: $d = 0.18$, $p = 0.009$) and spatial (long-distance connections, $d = 0.62$, $p < 0.001$) integration showed significantly higher cross-disorder involvement levels than expected for randomly distributed disease effects (indicated by an asterisk *, $p < 0.05$). Connections important for local clustering did not show higher than expected cross-disorder involvement ($p = 0.911$). Boxes indicate the interval between 25^{th} and 75^{th} percentiles (q_1 and q_3), whiskers indicate the interval between $q_1-1.5\times(q_3-q_1)$ and $q_3+1.5\times(q_3-q_1)$, white lines indicate median values and white circles indicate mean values.

Figure 3. Rich club organization. (a) Cross-disorder involvement of rich club connections (n = 88) was significantly higher as compared to the set of local connections (n = 751, $d = 0.43$, $p < 0.001$, one-sided permutation testing, 10,000 permutations) and higher than observed in the set of feeder connections (n = 321, $d = 0.28$, $p = 0.013$). Significant differences are indicated by * ($p < 0.05$) and boxes indicate the interval between 25^{th} and 75^{th} percentiles (q_1 and q_3), whiskers indicate the interval between $q_1-1.5\times(q_3-q_1)$ and $q_3+1.5\times(q_3-q_1)$, white lines indicate median values and white circles indicate mean values. (b) Hub regions (top 13% highest degree regions, 29 regions) are

colored in red. (c) Schematic representation of the human reference connectome with rich club connections (colored red), feeder connections (orange) and local connections (yellow).

Figure 4. Cross-disorder hyperconnectivity. (a) Lateral and medial view of left and right hemispheres showing region-wise cross-disorder hyperconnectivity. (b) Schematic representation of the human reference connectome with connections colored by cross-disorder hyperconnectivity. (c) Average cross-disorder hyperconnectivity of peripheral connections (blue) was compared with average cross-disorder hyperconnectivity in subject-label permuted cross-disorder involvement maps (grey). Peripheral connections, with low edge betweenness ($n = 290$, $d = 0.20$, $p = 0.002$, one-sided permutation testing, 10,000 permutations), small contribution to communicability ($d = 0.33$, $p < 0.001$) or short-distance connections ($d = 0.27$, $p < 0.001$) showed significantly higher cross-disorder hyperconnectivity as compared to effects in subject-label permuted null-models. Connections with low clustering did not show higher than expected cross-disorder hyperconnectivity ($p = 0.132$). (d) Cross-disorder hyperconnectivity of rich club, feeder and local connections. Local connections ($n = 751$) showed higher cross-disorder hyperconnectivity than feeder ($n = 321$, $d = 0.19$, $p = 0.003$, one-sided permutation testing, 10,000 permutations) or rich club connections ($n = 88$, $d = 0.29$, $p = 0.004$). (e) NBS analysis revealed two subnetworks with high cross-disorder involvement (NBS threshold 30%: $p = 0.026$; NBS threshold 40%: $p = 0.032$, one-sided permutation testing, 10,000 permutations). Brain regions (in blue) and schematic representation of the largest significant subnetwork (NBS threshold > 30%) are presented. Significant differences are indicated by * ($p < 0.05$) and boxes indicate the interval between 25th and 75th percentiles (q_1 and q_3), whiskers indicate the interval between $q_1-1.5\times(q_3-q_1)$ and $q_3+1.5\times(q_3-q_1)$, white lines indicate median values and white circles indicate mean values.

Figure 5. Overlap disorder disconnectivity with cross-disorder involvement map. For each disorder, the (weighted) disconnectivity of connections was compared between connections commonly affected across the 11 other disorders (affected in four or more disorders) and more disorder-specific connections (affected in zero, one or two disorders). Schizophrenia ($d = 0.77$, $p < 0.001$, two-sided permutation testing, 10,000 permutations, Bonferroni corrected for multiple testing across 12 disorders), PLS ($d = 0.71$, $p < 0.001$), ALS ($d = 0.71$, $p < 0.001$), bipolar disorder ($d = 0.42$, $p = 0.001$), obesity ($d = 0.33$, $p = 0.019$), Alzheimer's disease ($d = 0.31$, $p = 0.040$) and ASD ($d = 0.31$, $p = 0.035$) showed significantly higher disconnectivity in commonly affected connections. MCI ($p = 0.073$), ADHD ($p = 0.193$), PTSD ($p = 1$), MDD ($p = 0.767$) and OCD ($p = 0.152$) did not show significant differences.

Figure 6. Cross-comparison of cross-disorder gray matter abnormalities and region-wise cross-disorder white matter disconnectivity. (a) The vulnerability of 40 brain regions to white-matter disconnectivity and gray matter abnormalities are plotted with shaded areas indicating the top 5 regions with highest scores for either cross-disorder measure (y-axis starts at 0.015). **(b)** The average peak values of 40 brain regions to gray matter abnormalities are illustrated as provided by Crossley et al. (2014).

Tables

Table 1. Demographics after data quality control and matching.

			Age			Sex			
Dataset	Nr. con.	Nr. pat.	Con. mean (SD)	Pat. mean (SD)	P-value[a]	Con. male/female (%/%)	Pat. male/female (%/%)	P-value[b]	References
ADHD I	14	33	12.07 (2.48)	11.15 (2.54)	0.27	13/1 (92.9/.7.1)	27/6 (81.8/.18.2)	0.33	[49]
ALS	45	45	50.99 (19.10)	51.98 (15.98)	0.79	37/8 (82.2/.17.8)	33/12 (73.3/.26.7)	0.31	[74]
Alzheimer's disease I	20	20	61.65 (7.74)	66.00 (5.62)	0.05	8/12 (40.0/.60.0)	11/9 (55.0/.45.0)	0.34	[54,75]
Alzheimer's disease II	16	36	72.24 (4.54)	75.14 (8.90)	0.23	6/10 (37.5/.62.5)	21/15 (58.3/.41.7)	0.17	ADNI
ASD I	16	32	12.62 (1.86)	12.10 (2.48)	0.47	14/2 (87.5/.12.5)	27/5 (84.4/.15.6)	0.77	[49]
ASD II	22	32	13.37 (2.99)	12.97 (3.25)	0.65	20/2 (90.9/.9.1)	25/7 (78.1/.21.9)	0.22	ABIDE-II
ASD III	14	13	16.34 (3.31)	14.44 (3.52)	0.18	14/0 (100.0/.0.0)	13/0 (100.0/.0.0)	1.00	ABIDE-II
ASD IV	28	28	39.36 (15.04)	38.04 (15.78)	0.75	28/0 (100.0/.0.0)	28/0 (100.0/.0.0)	1.00	ABIDE-II
Bipolar disorder	82	82	45.18 (14.62)	45.86 (13.41)	0.76	42/40 (51.2/.48.8)	49/33 (59.8/.40.2)	0.27	[48]
MCI I	28	28	57.89 (12.22)	62.79 (7.81)	0.09	15/13 (53.6/.46.4)	19/9 (67.9/.32.1)	0.27	[54,75]
MCI II	17	95	72.80 (6.74)	72.48 (7.22)	0.87	8/9 (47.1/.52.9)	59/36 (62.1/.37.9)	0.24	ADNI
MDD	476	211	37.20 (11.78)	36.93 (12.15)	0.78	209/267 (43.9/.56.1)	104/107 (49.3/.50.7)	0.19	[50]
Obesity	32	29	23.53 (8.66)	26.45 (10.73)	0.25	15/17 (46.9/.53.1)	10/19 (34.5/.65.5)	0.33	[51]
OCD	42	36	31.81 (8.19)	31.50 (9.40)	0.88	18/24 (42.9/.57.1)	14/22 (38.9/.61.1)	0.72	[52]
PLS	32	32	59.18 (14.60)	59.93 (9.70)	0.81	19/13 (59.4/.40.6)	17/15 (53.1/.46.9)	0.61	[74]
PTSD I	25	46	36.92 (10.61)	37.66 (9.46)	0.77	25/0 (100.0/.0.0)	46/0 (100.0/.0.0)	1.00	[53]
PTSD II	40	40	69.86 (4.50)	68.04 (3.86)	0.06	40/0 (100.0/.0.0)	40/0 (100.0/.0.0)	1.00	DOD ADNI
Schizophrenia I	106	106	29.52 (7.63)	29.44 (7.41)	0.94	71/35 (67.0/.33.0)	82/24 (77.4/.22.6)	0.09	[47]
Schizophrenia II	24	24	31.79 (7.50)	31.21 (3.55)	0.74	17/7 (70.8/.29.2)	19/5 (79.2/.20.8)	0.50	[46]
Schizophrenia III	75	65	37.73 (11.97)	38.43 (13.47)	0.75	57/18 (76.0/.24.0)	51/14 (78.5/.21.5)	0.73	COBRE

[a] Independent-samples two-tailed t-test.

[b] Two-sided chi-squared test.

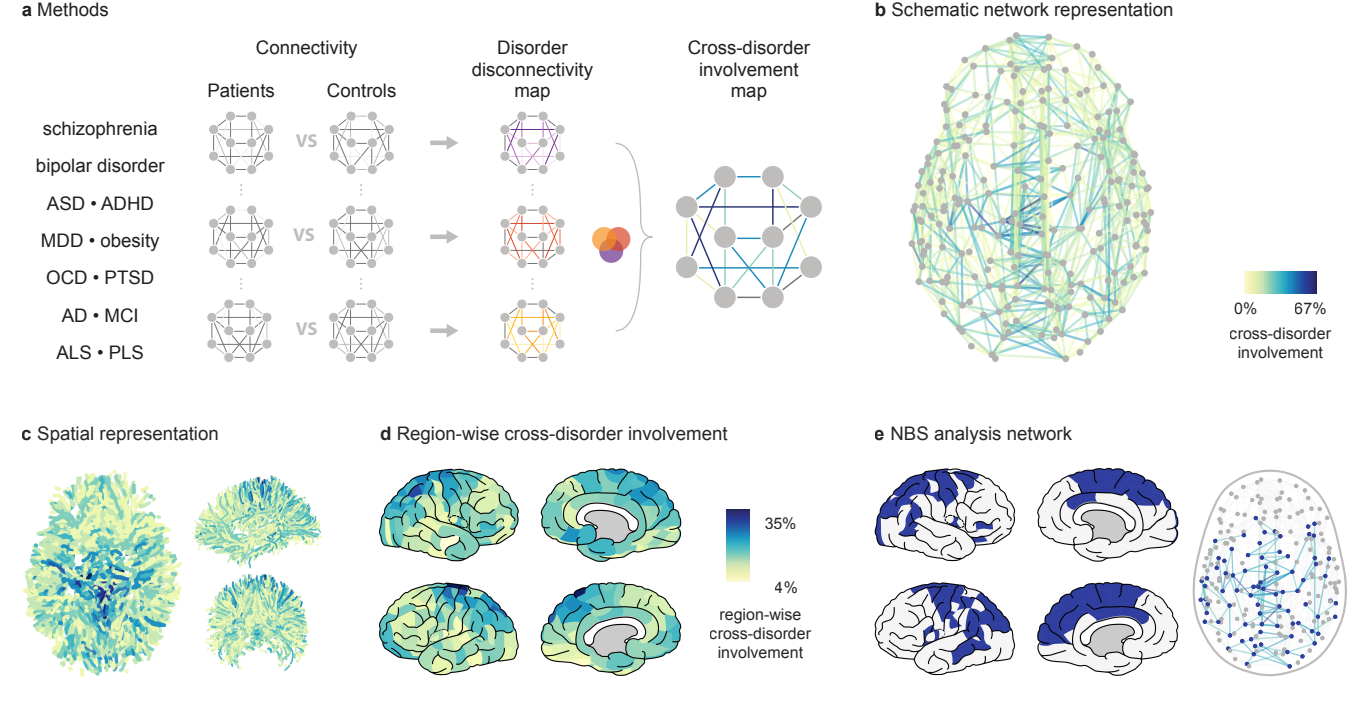
a Methods
Connectivity
Patients
Controls
Disorder disconnectivity map
Cross-disorder involvement map
schizophrenia
bipolar disorder
ASD • ADHD
MDD • obesity
OCD • PTSD
AD • MCI
ALS • PLS
VS
b Schematic network representation
0%
67%
cross-disorder involvement
c Spatial representation
d Region-wise cross-disorder involvement
35%
4%
region-wise cross-disorder involvement
e NBS analysis network

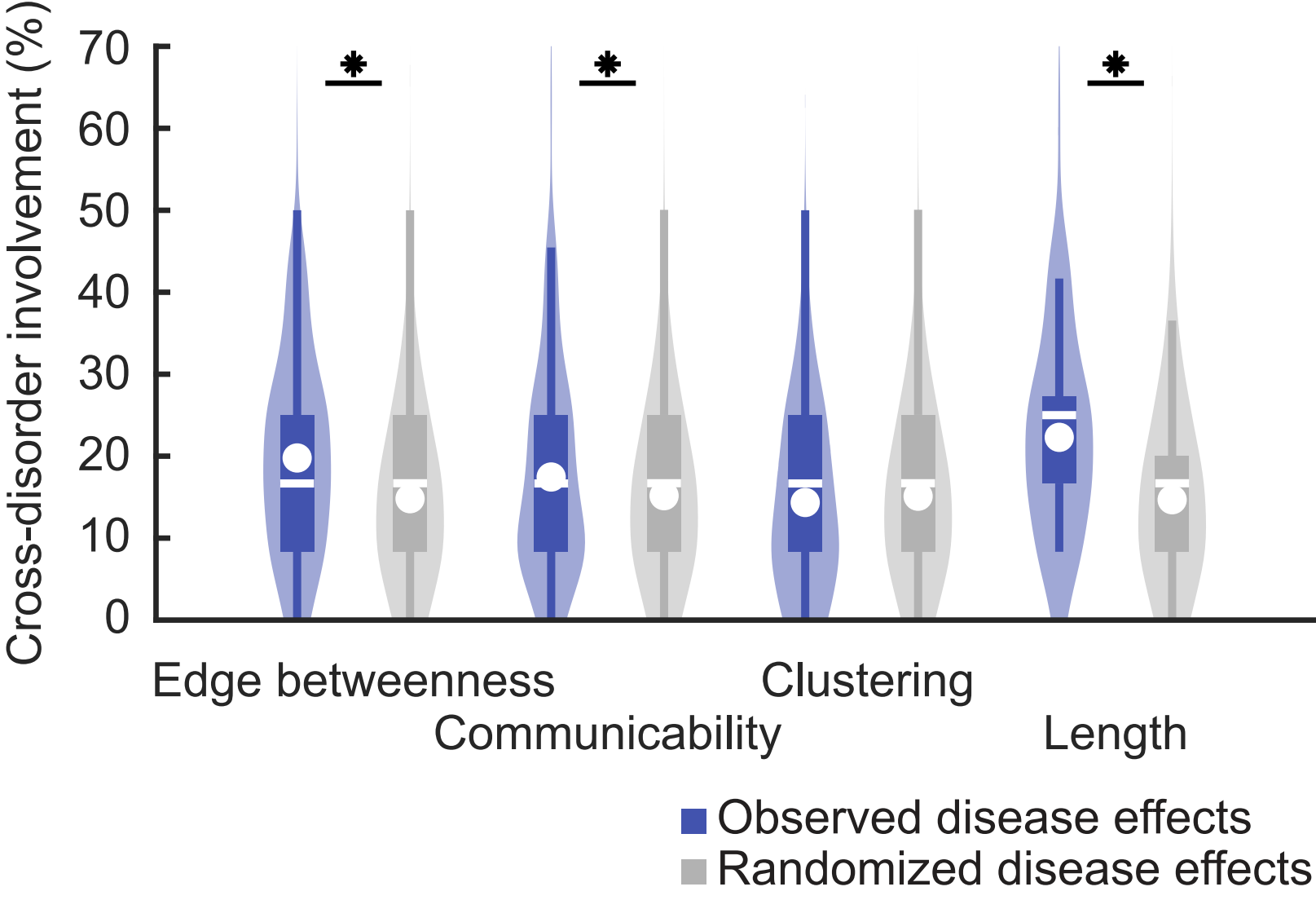
Cross-disorder involvement (%)
70
60
50
40
30
20
10
0
*
*
*
Edge betweenness
Communicability
Clustering
Length
Observed disease effects
Randomized disease effects

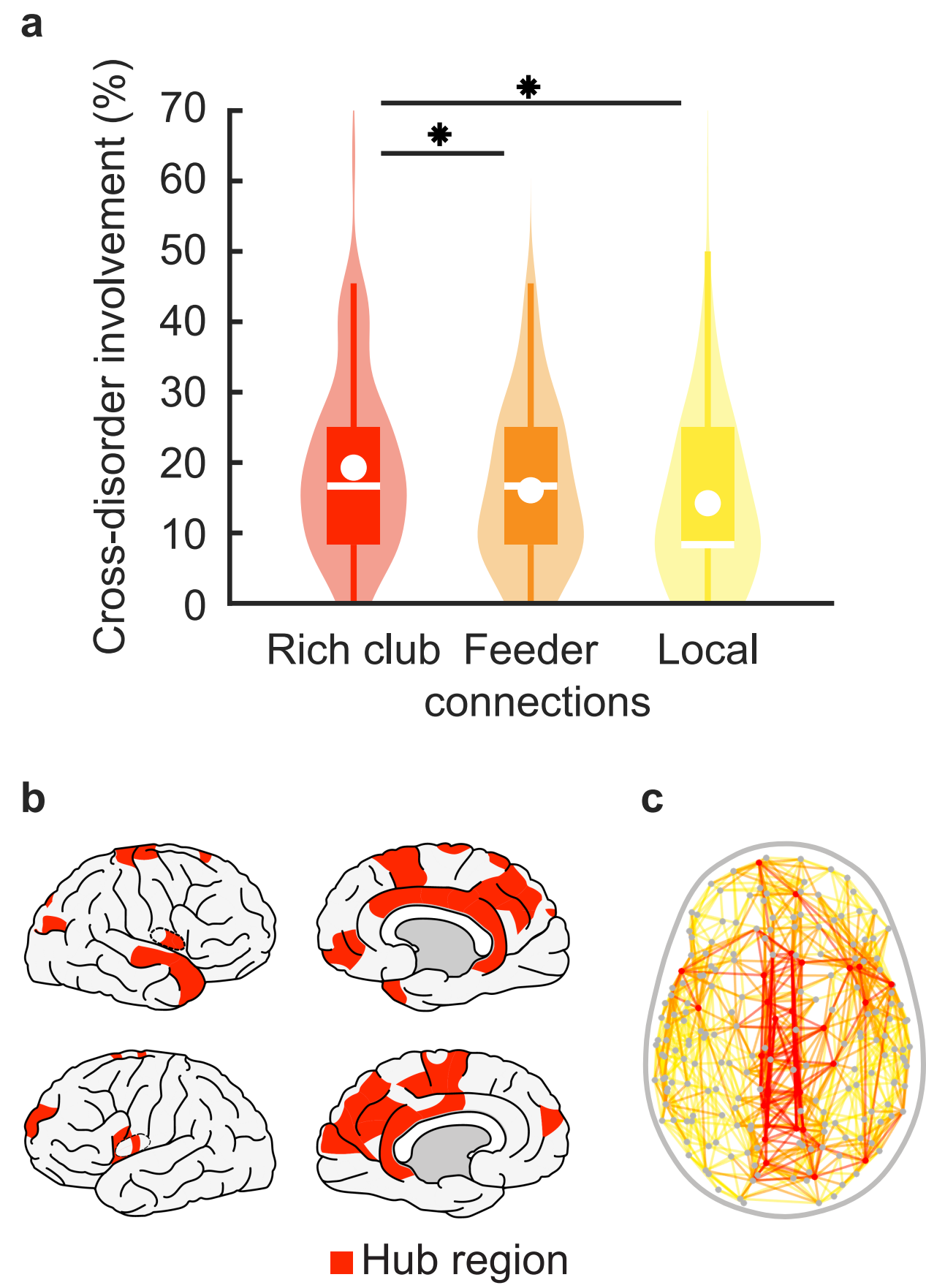
a
Cross-disorder involvement (%)
70
60
50
40
30
20
10
0
*
*
Rich club
Feeder connections
Local
b
c
Hub region

a Region-wise cross-disorder involvement

Hyperconnectivity

5% 34%

b Network representation

0% 67%

c Peripheral connections

Cross-disorder involvement (%)

Edge betweenness
Communicability
Clustering
Length

d Rich club organization

Cross-disorder involvement (%)

Rich club Feeder Local

e NBS analysis network

Number of regions in greatest component

Cross-disorder involvement threshold

Cross-disorder involvement threshold 30% (p = 0.026)

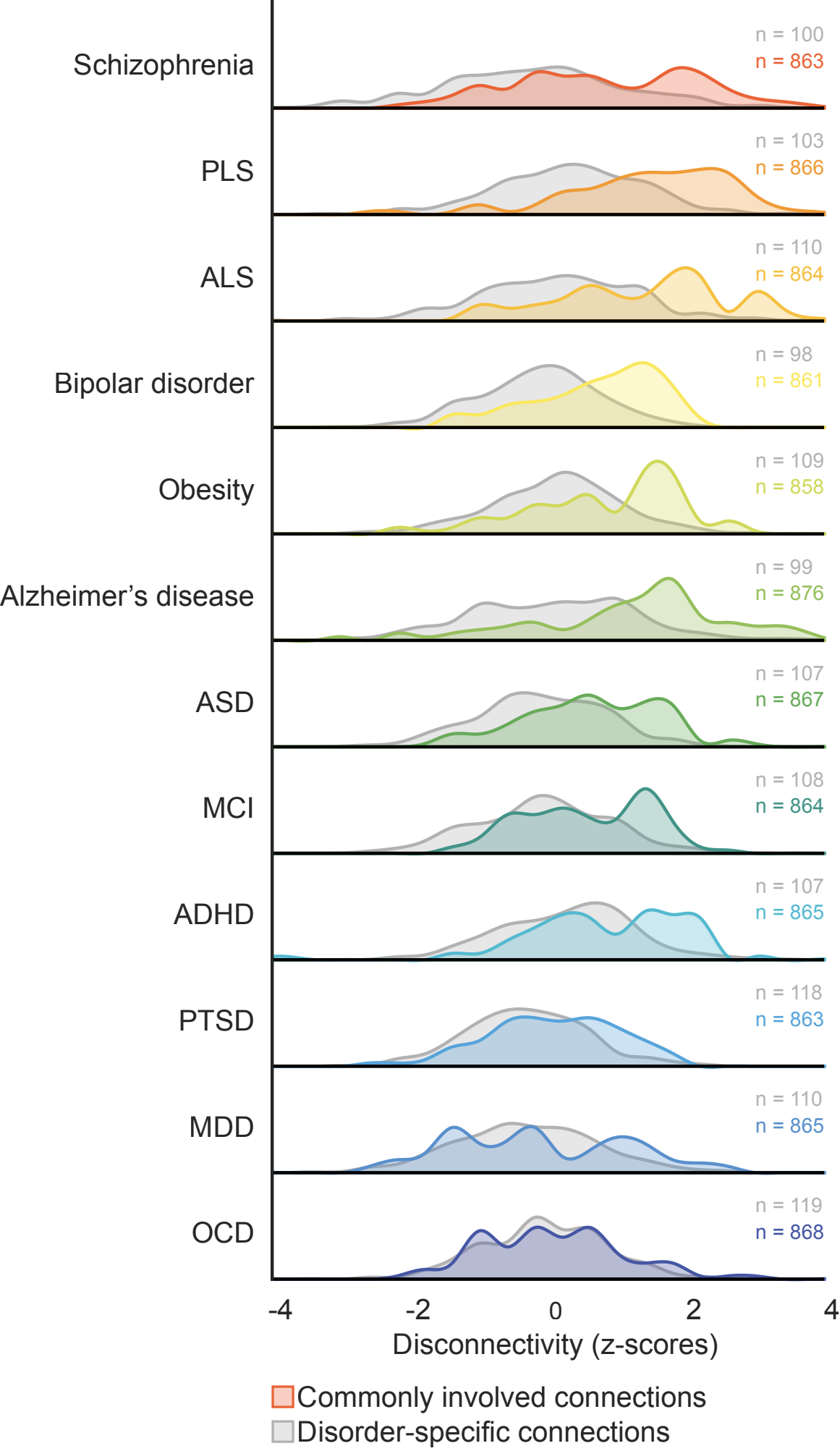
Schizophrenia
n = 100
n = 863
PLS
n = 103
n = 866
ALS
n = 110
n = 864
Bipolar disorder
n = 98
n = 861
Obesity
n = 109
n = 858
Alzheimer's disease
n = 99
n = 876
ASD
n = 107
n = 867
MCI
n = 108
n = 864
ADHD
n = 107
n = 865
PTSD
n = 118
n = 863
MDD
n = 110
n = 865
OCD
n = 119
n = 868
-4
-2
0
2
4
Disconnectivity (z-scores)
Commonly involved connections
Disorder-specific connections

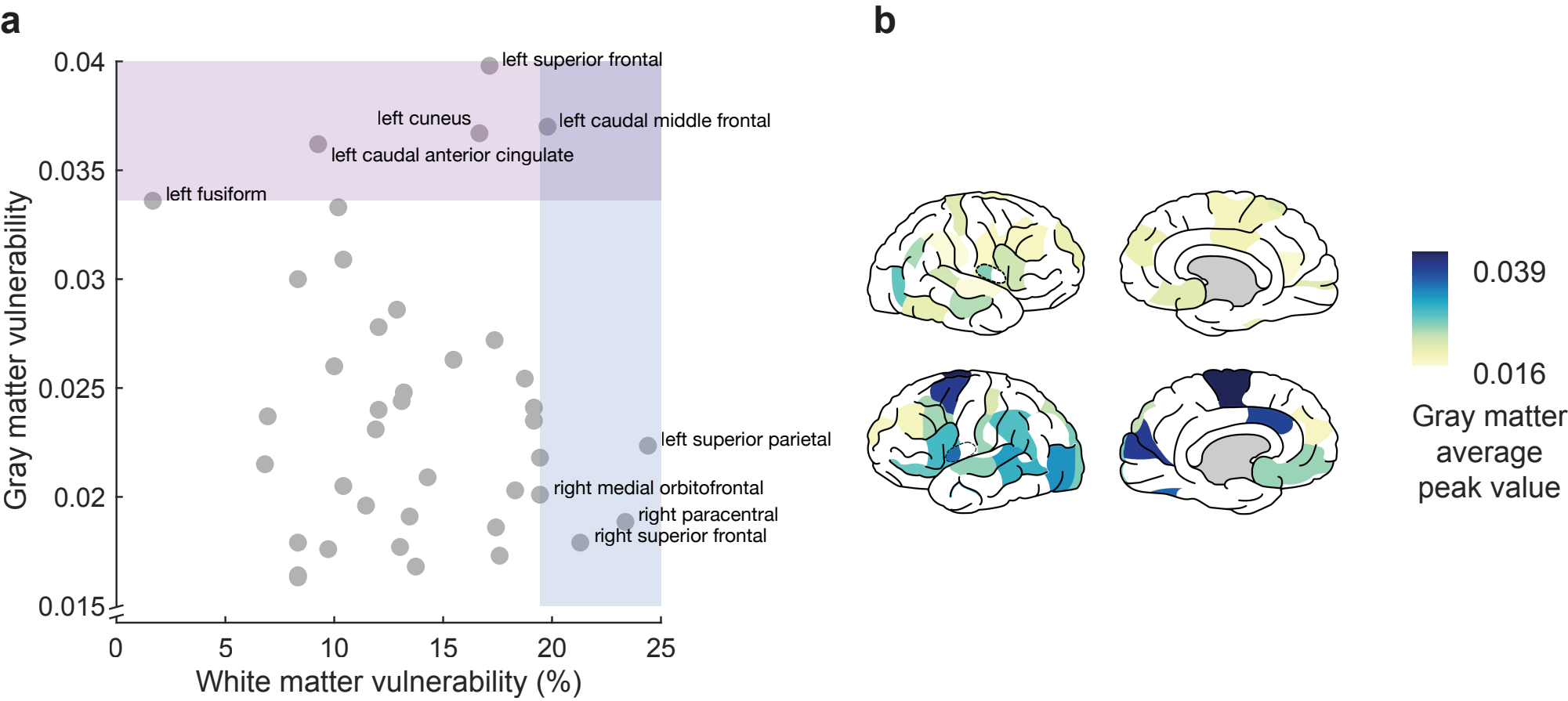
a
b
0.04
0.035
0.03
0.025
0.02
0.015
Gray matter vulnerability
0
5
10
15
20
25
White matter vulnerability (%)
left superior frontal
left cuneus
left caudal middle frontal
left caudal anterior cingulate
left fusiform
left superior parietal
right medial orbitofrontal
right paracentral
right superior frontal
0.039
0.016
Gray matter average peak value